Inelastic neutron scattering study on the noncentrosymmetric compounds $PrCuAl_3$ and $NdCuAl_3$

D. T. Adroja* and V. K. Anand†

ISIS Facility, Rutherford Appleton Laboratory, Chilton, Didcot, Oxon, OX11 0QX, United Kingdom

(Received 20 June 2012; published 4 September 2012)

We present the structural, magnetic, thermal, and transport properties of two noncentrosymmetric compounds $PrCuAl_3$ and $NdCuAl_3$ from the magnetic susceptibility $\chi(T)$, isothermal magnetization $M(H)$, specific heat $C_p(T)$, neutron diffraction, and inelastic neutron scattering (INS) investigations. Our x-ray diffraction and neutron diffraction data confirm that both $PrCuAl_3$ and $NdCuAl_3$ crystallize in $BaNiSn_3$-type noncentrosymmetric tetragonal crystal structure. While $PrCuAl_3$ remains paramagnetic down to 1.8 K, a clear evidence for an antiferromagnetic ordering below 2.35 K in $NdCuAl_3$ is inferred from the $\chi(T)$ and $C_p(T)$. The absence of magnetic order in $PrCuAl_3$ can be attributed to crystal electric field (CEF) effect. The $C_p(T)$ data suggest the CEF ground state to be a nonmagnetic singlet in $PrCuAl_3$ and a magnetic doublet in $NdCuAl_3$, which are further confirmed by the INS study. The INS spectra reveal two sharp CEF excitations near 2 and 9 meV in $PrCuAl_3$, and four CEF excitations near 1.4, 3.2, 8.9, and 10.9 meV in $NdCuAl_3$. An analysis of the INS data of both the compounds is presented based on the CEF model, which accounts for the observed position and intensity of all the observed CEF excitations. The ground state wave functions have been evaluated from the analysis of the INS data.

DOI: 10.1103/PhysRevB.86.104404 PACS number(s): 78.70.Nx, 71.70.Ch, 75.50.Ee, 65.40.Ba

I. INTRODUCTION

Recently the intermetallic compounds that lack inversion symmetry in their crystal structure have attracted considerable attention and lead to a very important class of material: noncentrosymmetric superconductors—the lack of inversion symmetry introduces an antisymmetric spin-orbit coupling (ASOC) which plays a key role in dictating the normal and superconducting state properties of such materials.[1–7] ASOC removes the spin degeneracy of conduction band electrons and leads to parity mixing. As a consequence the Cooper pair wave function of noncentrosymmetric superconductors consists of a combination of *spin-singlet* and *spin-triplet* states. $BaNiSn_3$-type crystal structure (space group $I4\,mm$) is one such noncentrosymmetric structure which lacks inversion symmetry along the c axis. Compounds crystallizing with $BaNiSn_3$-type crystal structure such as heavy fermion antiferromagnets $CeRhSi_3$, $CeIrSi_3$, and $CeCoGe_3$ have been found to show unconventional superconductivity (SC) under the application of pressure which is very rich in physics due to its proximity to a magnetic quantum critical point (QCP).[8–19] However, despite the extensive efforts very little is known about the superconducting order parameter and primary mechanism activating unconventional SC in such noncentrosymmetric systems.

In our effort to further the research on noncentrosymmetric systems we started working on compounds that crystallize with $BaNiSn_3$-type crystal structure which should enable us to explore the relationship between the physical properties and inversion symmetry in general. Recently we have reported our investigations on noncentrosymmetric superconductor $LaRhSi_3$ in which we observed an exponential evolution of Sommerfeld coefficient γ with magnetic field which we believe to be due to the reinforcement of ASOC with magnetic field.[20] Another noncentrosymmetric compound $PrRuSi_3$ is found to exhibit spin-glass behavior.[21] Our inelastic neutron scattering study revealed that $PrRuSi_3$ has a singlet ground state and exhibits an induced moment magnetism. Thus the dynamic fluctuations of crystal field levels that destabilizes the induced moment magnetism is believed to be responsible for the spin-glass behavior in $PrRuSi_3$.[21] Here we report the magnetic and transport properties of two noncentrosymmetric ternary intermetallic compounds $PrCuAl_3$ and $NdCuAl_3$ which are reported to crystallize with $BaNiSn_3$-type tetragonal crystal structure.[22] From a preliminary magnetic measurement $NdCuAl_3$ is reported to exhibit ferromagnetic behavior below ~5 K.[22] The Ce-analog $CeCuAl_3$ which also crystallizes in the same structure is a heavy fermion Kondo lattice system situated close to a quantum critical point that undergoes an antiferromagnetic ordering below ~3 K with Kondo temperature $T_K \sim 10$ K at ambient pressure.[23–26] The high pressure study up to 80 kbar could not induce superconductivity in this compound.[27–29]

Recently we have performed inelastic neutron scattering (INS) experiment on $CeCuAl_3$ and found the presence of three magnetic/crystal electric field (CEF) excitations in INS spectra compared to two CEF excitations expected from Kramers theorem (in the paramagnetic state).[30] This provides strong evidence for the CEF-phonon coupling in this compound. The Kramer's degeneracy theorem predicts that in Ce compounds, having odd numbers of $4f$ electron, there ought not to be more than two CEF excitations from the $J = 5/2$ ground state of Ce^{3+} ion in the paramagnetic state. A theoretical model based on CEF-phonon coupling which explains the observed INS spectra very well suggests that the magnetic and transport properties of $CeCuAl_3$ are strongly influenced by the presence of vibrons.[30] Therefore to understand and explore the role of vibrons in $CeCuAl_3$ we have investigated the Pr and Nd analogs of this compound, i.e., $PrCuAl_3$ and $NdCuAl_3$. None of them were found to exhibit superconductivity at ambient pressure. The magnetic susceptibility $\chi(T)$ and specific heat $C_p(T)$ data show that $PrCuAl_3$ remains paramagnetic down to 1.8 K with a CEF-split singlet ground state, and $NdCuAl_3$ orders antiferromagnetically below 2.3 K with a doublet ground state. Our inelastic neutron scattering study clearly reveals two sharp CEF excitations near 2 and 9 meV in the INS spectra of

$PrCuAl_3$, and four CEF excitations near 1.4, 3.2, 8.9, and 10.9 meV in $NdCuAl_3$ which have been analyzed by a model based on the crystal electric field.

II. EXPERIMENTAL

The polycrystalline samples of $PrCuAl_3$ and $NdCuAl_3$ were prepared by the standard arc melting technique of stoichiometric mixture of high purity elements (Pr, Nd: 99.9%, Cu: 99.99%, Al: 99.99%) on a water cooled copper hearth under the titanium gettered inert argon atmosphere. In order to homogenize and improve the reaction among the constituent elements, the samples were flipped and remelted five times. Further, to improve the phase formation and homogeneity the as-obtained samples were annealed at 900 °C for a week under dynamic vacuum. The crystal structure was determined through the powder x-ray diffraction (XRD) using the Cu K_α radiation, and the phase purity of samples was checked by scanning electron microscopy (SEM). The stoichiometry was checked by the energy dispersive x-ray (EDX) analysis. The magnetization was measured by using a commercial superconducting quantum interference device (SQUID) magnetometer (MPMS, Quantum Design). For the specific heat measurement we used a physical properties measurement system (PPMS, Quantum Design) employing the relaxation method. The neutron diffraction experiment was performed on the powdered sample of $NdCuAl_3$ at room temperature using the ROTAX diffractometer at the ISIS facility of the Rutherford Appleton Laboratory, Didcot, UK. The inelastic neutron scattering (INS) measurements were performed on the powdered samples (filled in a thin Al-foil envelop) using the HET time-of-flight chopper spectrometer at ISIS. The low temperature down to 4.5 K was obtained by cooling the samples with He-exchange gas inside a top-loading closed-cycle refrigerator (TCCR). The INS measurements were performed with incident neutron energy E_i of 11 and 20 meV.

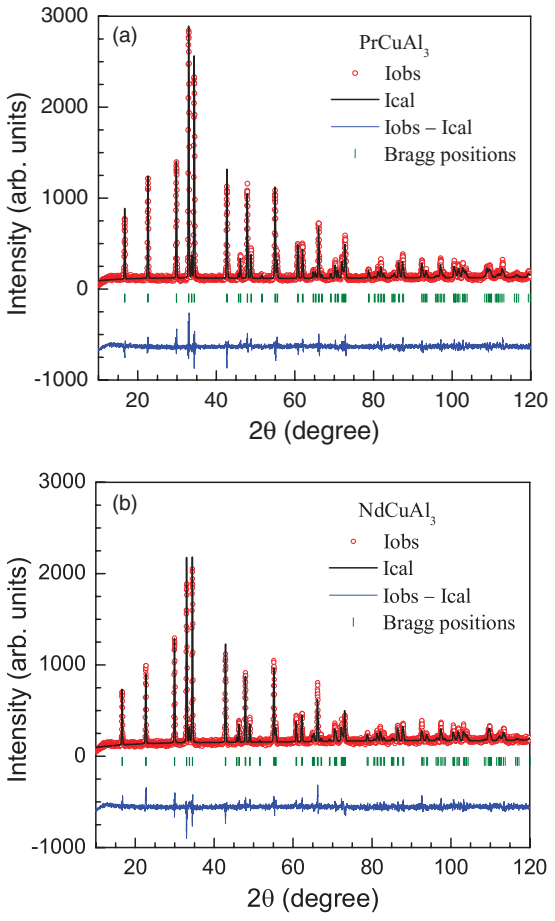

FIG. 1. (Color online) The powder x-ray diffraction pattern of (a) $PrCuAl_3$ and (b) $NdCuAl_3$ recorded at room temperature. The solid lines through the experimental points are the FullProf Rietveld refinement profiles calculated for $BaNiSn_3$-type tetragonal (space group $I4\,mm$) structural model. The vertical short columns indicate the Bragg peak positions. The lowermost curves represent the difference between the experimental and calculated intensities.

III. RESULTS AND DISCUSSION

A. Crystallography

The crystal structures of $PrCuAl_3$ and $NdCuAl_3$ were determined by the Rietveld refinement of powder x-ray diffraction and neutron diffraction data, both of which indicate an essentially single phase nature of the samples and confirm the $BaNiSn_3$-type tetragonal structures (space group $I4\,mm$) for $PrCuAl_3$ and $NdCuAl_3$. The XRD pattern for $PrCuAl_3$ and $NdCuAl_3$, and the neutron diffraction pattern for $NdCuAl_3$ recorded at room temperature together with the structural Rietveld refinement profiles for $BaNiSn_3$-type tetragonal structure are shown in Figs. 1 and 2. The results obtained from the least squares refinements of XRD and neutron diffraction data are listed in Tables I and II. While refining the occupancies of atoms were kept fixed to unity as the small variation in occupancy did not improve the quality of fits. For the same reason the thermal parameters B were also set to $B = 0$ during the refinement of XRD data. The lattice parameters obtained from the neutron diffraction data for $NdCuAl_3$ are

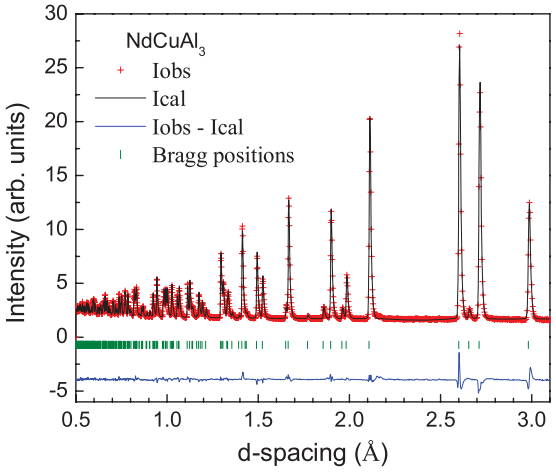

FIG. 2. (Color online) The neutron diffraction pattern of $NdCuAl_3$ recorded at room temperature. The solid line through the experimental points is the GSAS Rietveld refinement profile calculated for the $BaNiSn_3$-type tetragonal (space group $I4\,mm$) structural model. The vertical short columns indicate the Bragg peak positions. The lowermost curve represents the difference between the experimental and calculated intensities.

TABLE I. Crystallographic parameters of $PrCuAl_3$ and $NdCuAl_3$ determined from the structural Rietveld refinement of room temperature x-ray diffraction and neutron diffraction data.

	$PrCuAl_3$	$NdCuAl_3$	
Structure	$BaNiSn_3$ type tetragonal	$BaNiSn_3$ type tetragonal	
Space group	$I4\,mm$	$I4\,mm$	
Lattice parameters			
a (Å)	4.2357(2)	4.2191(2)	x-ray
		4.2191(4)	neutron
c (Å)	10.6308(4)	10.6305(5)	x-ray
		10.6264(9)	neutron
V_{cell}(Å^3)	190.73(1)	189.24(1)	x-ray
		189.16(5)	neutron
Refinement quality			
χ^2	2.23		
R_p (%)	8.95	2.93	
R_{wp} (%)	11.5	3.79	

in very good agreement with those obtained from the powder x-ray diffraction (see Table I) and agree with the literature values.[22] The lattice parameters of $PrCuAl_3$ also agree well with reported values.[22] Further, the single phase nature and the homogeneity of both the samples were confirmed by the high resolution SEM images and EDX. The EDX composition analysis confirmed the desired stoichiometry of 1:1:3 for both the compounds.

B. Magnetic susceptibility and magnetization studies

The magnetic susceptibility χ as a function of temperature T for $PrCuAl_3$ is shown in Fig. 3(a). The $\chi(T)$ data of $PrCuAl_3$ do not show any transition except a weak anomaly near 4.7 K as can be seen from the insets of Fig. 3(a). No change is observed in the anomaly with an increase in applied field. The zero-field-cooled (ZFC) and field-cooled (FC) χ measured at 0.01 T do not show any hysteresis below 4.7 K [the upper inset of Fig. 3(a)]. The nature of weak anomaly near 4.7 K is not clear. This could be due to the presence of a small amount of spurious phase that was not detected by XRD or SEM. However, we cannot completely rule out that this weak

TABLE II. Atomic coordinates obtained from the structural Rietveld refinement of room temperature x-ray diffraction data of $PrCuAl_3$ and neutron diffraction data of $NdCuAl_3$.

Atom	Wyckoff symbol	x	y	z	U_{iso}(Å^2)
$PrCuAl_3$					
Pr	2a	0	0	0	
Cu	2a	0	0	0.635(1)	
Al1	2a	0	0	0.405(1)	
Al2	4b	0	1/2	0.248(2)	
$NdCuAl_3$					
Nd	2a	0	0	0	0.0048(3)
Cu	2a	0	0	0.6323(2)	0.0105(4)
Al1	2a	0	0	0.4087(3)	0.0096(7)
Al2	4b	0	1/2	0.2502(3)	0.0105(5)

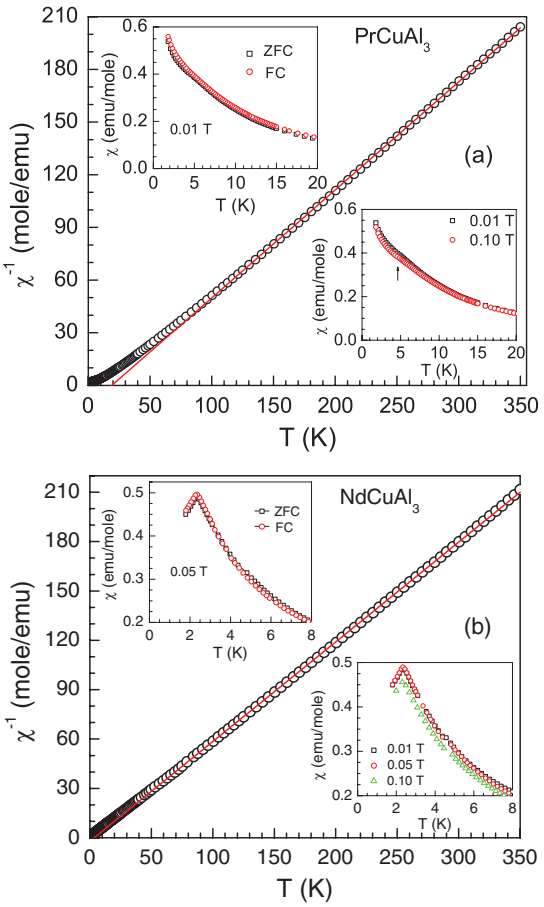

FIG. 3. (Color online) The temperature T dependence of dc magnetic susceptibility χ of (a) $PrCuAl_3$ and (b) $NdCuAl_3$, plotted as $\chi^{-1}(T)$ in the temperature range 2–350 K, measured in an applied field $H = 0.1$ T. The solid lines represent the fit of $\chi^{-1}(T)$ data by Curie-Weiss behavior. The lower insets show the low-T $\chi(T)$ data measured at different H. The upper insets show the zero-field-cooled (ZFC) and field-cooled (FC) χ.

anomaly in $\chi(T)$ is intrinsic to the susceptibility of $PrCuAl_3$. At high temperatures the susceptibility data exhibit a Curie-Weiss behavior, $\chi(T) = C/(T - \theta_p)$, where C is the Curie constant and θ_p is the Curie-Weiss temperature. A linear fit of the inverse magnetic susceptibility data, $\chi^{-1}(T)$, measured at $H = 0.1$ T in the temperature range 100 K $\leqslant T \leqslant$ 350 K [the solid line in Fig. 3(a)] yields $C = 0.616(1)$ and Curie-Weiss temperature $\theta_p = +19(1)$ K. A positive θ_p may suggest the presence of ferromagnetic fluctuations. From C we obtain an effective moment $\mu_{eff} = 3.60(1)\,\mu_B$ which is very close to the theoretically expected value of effective moment for Pr^{3+} ions ($3.58\,\mu_B$).

The isothermal magnetization M as a function of applied magnetic field H for $PrCuAl_3$ is shown in Fig. 4(a). The $M(H)$ isotherm at 2 K exhibits slight nonlinearity with magnetic field [Fig. 4(a)] which can be due to the presence of the magnetic fluctuations and/or crystal field effects. No hysteresis is observed in increasing and decreasing cycles of H in $M(H)$ isotherm at 2 K. At higher temperatures (e.g., at 20 K and 50 K) the $M(H)$ isotherms exhibit an almost linear field dependence, however with a reduced saturation magnetization. At 2 K and 7 T, the magnetization attains a value of $\sim$2.05 μ_B,

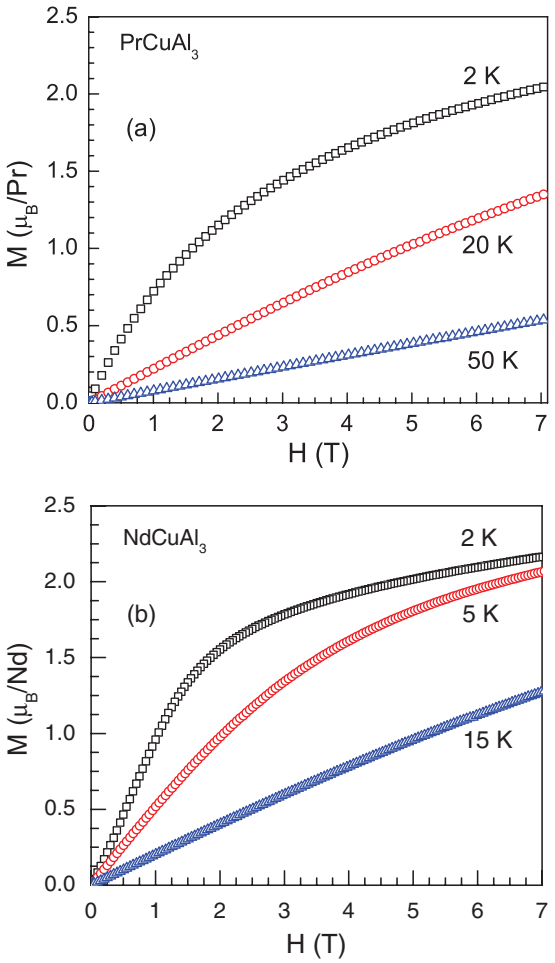

FIG. 4. (Color online) The magnetic field H dependence of isothermal magnetization M of (a) $PrCuAl_3$ and (b) $NdCuAl_3$ measured at the indicated temperatures.

which is much lower than the theoretical value of saturation magnetization for Pr^{3+} ions ($M_s = g_J J \mu_B = 3.2\,\mu_B$).

The $\chi(T)$ data for $NdCuAl_3$ are shown in Fig. 3(b). The low temperature $\chi(T)$ data of $NdCuAl_3$ measured at different fields show a well defined peak at 2.35 K due to a magnetic phase transition [see the insets of Fig. 3(b)]. The magnetic transition at 2.35 K seems to be of antiferromagnetic nature in contrast to the reported ferromagnetic behavior below ~5 K.[22] In Ref. 22 no $\chi(T)$ data were presented, therefore we could not present the comparison. In order to understand the nature of transition we measured the ZFC and FC χ which are shown in the upper inset of Fig. 3(b). No hysteresis is observed in ZFC and FC $\chi(T)$, which supports the antiferromagnetic behavior in $NdCuAl_3$. The high temperature $\chi(T)$ is consistent with the Curie-Weiss behavior. On fitting the $\chi^{-1}(T)$ data measured at $H = 0.1$ T in the temperature range 50 K $\leqslant T \leqslant$ 350 K [the solid line in Fig. 3(b)] we obtain $\mu_{\rm eff} = 3.63(1)\,\mu_B$ and $\theta_p = +3.5(1)$ K. The value of effective moment obtained is very close to the theoretical value of effective moment for Nd^{3+} ions (3.58 μ_B).

The $M(H)$ data for $NdCuAl_3$ are shown in Fig. 4(b). In the ordered state (at 2 K) the isothermal magnetization M initially increases rapidly with magnetic field up to $H \sim$ 1.4 T followed by a slow increase afterwards and attains a value of $\sim 2.17\,\mu_B$ at $H = 7$ T, which is much lower than the theoretically expected value of saturation magnetization for Nd^{3+} ions ($M_s = 3.2\,\mu_B$). A slight nonlinearity is observed in magnetization even above the transition temperature (at 5 K), which can be attributed to the presence of short range correlations and/or crystal field effects. At 15 K $M(H)$ isotherm is almost linear in H. Further, the $M(H)$ isotherm at 2 K is found to exhibit no hysteresis in increasing and decreasing cycles of H as usually one would expect for a ferromagnetic system. Moreover the $M(H)$ also does not reveal the appearance of spontaneous magnetization, i.e., the sharp jump in $M(H)$ at an extremely low field which is typically observed in ferromagnetic systems. Thus, the magnetic field dependence of M also indicates an antiferromagnetic ground state in $NdCuAl_3$.

C. Specific heat studies

The specific heat data $C_p(T)$ of $LaCuAl_3$, $PrCuAl_3$, and $NdCuAl_3$ measured at constant pressure p are shown in Fig. 5.

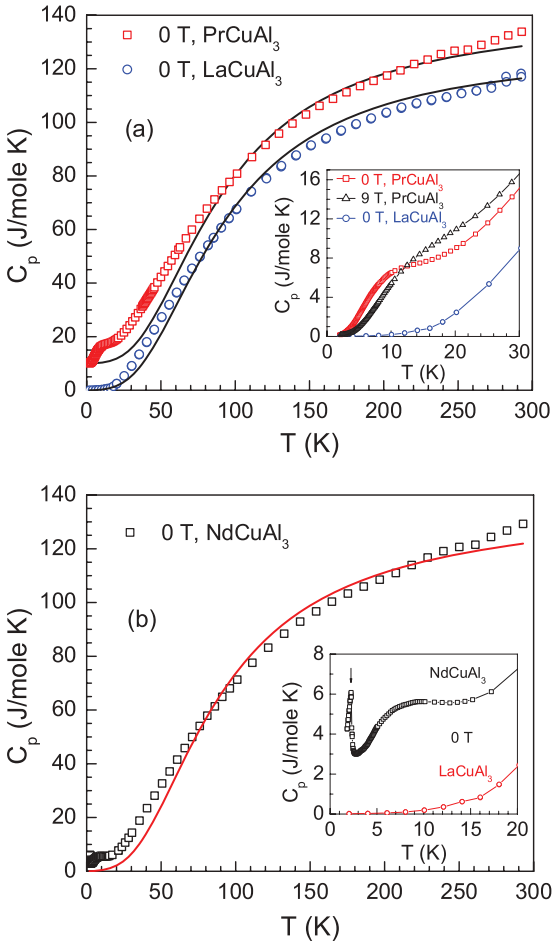

FIG. 5. (Color online) The temperature T dependence of zero field specific heat C_p of (a) $PrCuAl_3$ and (b) $NdCuAl_3$ measured in the temperature range 1.8–300 K. For clarity the $C_p(T)$ data of $PrCuAl_3$ in (a) are shifted up by 10 J/mole K. The solid curves represent the fit of $C_p(T)$ data by Debye model of lattice heat capacity. The insets show the expanded view of low-T $C_p(T)$ data at different applied magnetic fields. The $C_p(T)$ data of nonmagnetic reference compound $LaCuAl_3$ are also shown.

While there is no sharp anomaly in the specific heat of $LaCuAl_3$ and $PrCuAl_3$ corresponding to magnetic order or superconducting transition down to 1.8 K, we clearly see a sharp and well defined λ-type peak at 2.25 K in the low temperature $C_p(T)$ data of $NdCuAl_3$ [inset of Fig. 5(b)]. The specific heat transition at 2.25 K confirms the intrinsic nature of antiferromagnetic order in $NdCuAl_3$ as inferred from the magnetic susceptibility data. The broad anomalies observed in the low temperature specific heat of $PrCuAl_3$ and $NdCuAl_3$ reflect the presence of crystal field effect in these compounds. The $C_p(T,H)$ data of $PrCuAl_3$ measured in an applied magnetic field of 9 T [inset of Fig. 5(a)] indicate that the Schottky type CEF anomaly becomes more broad and shifts towards the higher temperature.

The $C_p(T,H)$ data of $NdCuAl_3$ measured in different applied magnetic fields up to 2 T are shown in Fig. 6. It is seen from Fig. 6(a) that with the application of field the Schottky type CEF anomaly tends to become broader, however shifts towards the lower temperature. This decrease of CEF anomaly temperature T_{CEF} in $C_p(T,H)$ of $NdCuAl_3$ contrasts the above observation of increase in T_{CEF} for $PrCuAl_3$. Thus we see that while with the field the CEF splitting between the ground state and first excited state in $PrCuAl_3$ tends to increase, in $NdCuAl_3$ the CEF splitting energy between the ground state and first excited state tends to decrease. The difference could be associated with the singlet ground state in $PrCuAl_3$ that will not change in applied field, whereas the doublet ground state (as well as first excited state) in $NdCuAl_3$ will split in applied magnetic field. Further, we see that with the application of field the λ-type anomaly associated with the magnetic ordering shifts towards the lower temperature, characterizing the magnetic order to be antiferromagnetic type in contrast to the previously reported ferromagnetic behavior.[22] It is observed that at $H = 0.25$ T there appears another peak at $T_t = 2.15$ K in $C_p(T,H)$ due to a field induced spin reorientation in addition to the peak at T_N [see Fig. 6(b)]. The T_t is found to exhibit stronger H dependence than T_N. At $H = 0.35$ T T_t shifts to 2.05 K from $T_t = 2.15$ K at $H = 0.25$ T, and at $H = 0.5$ T T_t moves to a temperature below 1.8 K, though a tail of T_t is clearly seen at $H = 0.5$ T. At further higher fields T_t is completely suppressed to a temperature below 1.8 K. At $H = 1$ T T_N shifts to 2.02 K, and at fields 1.5 and 2.0 T no anomaly is observed in $C_p(T,H)$ above 1.8 K. The observation of a field induced transition at T_t in $C_p(T,H)$ suggests a complex magnetic structure in $NdCuAl_3$ and may be related to the weak slope change in $M(H)$ curve at 2 K below $H = 0.5$ T likely due to the spin-flop/metamagnetic transition which is not very pronounced in polycrystalline average. A single crystal study should be desirable for a clear picture.

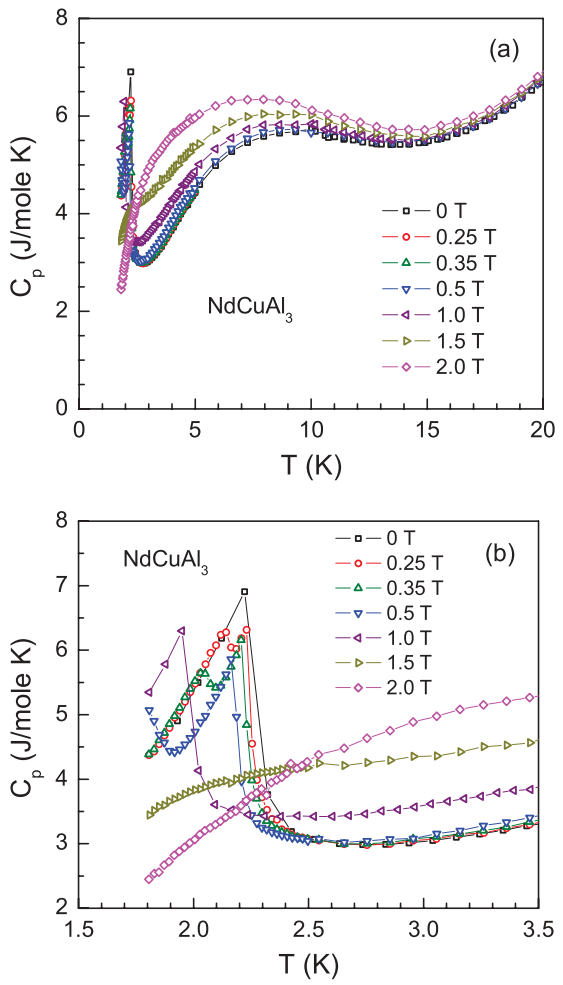

FIG. 6. (Color online) (a) The temperature T dependence of low-T specific heat C_p of $NdCuAl_3$ measured in different applied field H. (b) Expanded view of $C_p(T,H)$ near T_N.

The low temperature specific heat data of $LaCuAl_3$ are well represented by[31]

$$C_p(T) = \gamma T + \beta T^3, \tag{1}$$

where the first term represents the electronic contribution to specific heat and the second term is the lattice contribution given by Debye T^3 law. A fit of $C_p(T)$ data of $LaCuAl_3$ by Eq. (1) gives the Sommerfeld coefficient $\gamma = 4.1(4)$ mJ/mole K^2 and $\beta = 1.42(7) \times 10^{-4}$ J/mole K^4. However, the $C_p(T)$ data of $PrCuAl_3$ and $NdCuAl_3$ could not be described by Eq. (1). The C_p/T value of ~76 mJ/mole K^2 at 1.9 K clearly reflects a slightly enhanced γ in $PrCuAl_3$ due to the crystal field effect. Whereas for $NdCuAl_3$ the presence of magnetic order and CEF makes it difficult to estimate the value of specific heat coefficient γ. Further, we estimated the Debye temperature Θ_D from β using the relation[31]

$$\Theta_D = \left(\frac{12\pi^4 nR}{5\beta}\right)^{1/3}, \tag{2}$$

where R is the molar gas constant and n is the number of atoms per formula unit (f.u.) which is 5 for $LaCuAl_3$. Thus we obtain $\Theta_D = 409(6)$ K for $LaCuAl_3$.

At room temperature (300 K) the specific heat is found to attain a value of ~117 J/mole K for $LaCuAl_3$, ~124 J/mole K for $PrCuAl_3$, and ~129 J/mole K for $NdCuAl_3$ which are close to the expected classical Dulong-Petit value of $C_V = 3nR = 15R = 124.7$ J/mole K. The high temperature $C_p(T)$ data of all the compounds could be analyzed within the framework of Debye model of lattice heat capacity that describes the lattice heat capacity due to the acoustic phonons and is given by[32]

$$C_{V\,\mathrm{Debye}}(T) = 9nR\left(\frac{T}{\Theta_D}\right)^3 \int_0^{\Theta_D/T} \frac{x^4 e^x}{(e^x - 1)^2}\, dx. \tag{3}$$

The $C_p(T)$ data were fitted by

$$C_p(T) = C_{V\,\mathrm{Debye}}(T) + \gamma T \quad (4)$$

in the whole temperature range. The least squares fit of $C_p(T)$ data by Eqs. (3) and (4) are shown by the solid curves in Fig. 5. For $C_{V\,\mathrm{Debye}}(T)$ we used the analytic Padé approximant fitting function.[33] For $LaCuAl_3$ while fitting the $C_p(T)$ data we fixed the γ to the value determined above, thus the only fitting parameter was Θ_D which was found to be $\Theta_D = 371(3)$ K which is slightly different from the above determined value of $\Theta_D = 409(6)$ K from low-T $C_p(T)$ data. However, for $PrCuAl_3$ and $NdCuAl_3$ we kept γ as an adjustable parameter. The best fits were obtained with $\gamma = 15(3)$ mJ/mole K^2 and $\Theta_D = 366(6)$ K for $PrCuAl_3$ and $\gamma = 20(4)$ mJ/mole K^2 and $\Theta_D = 354(5)$ K for $NdCuAl_3$. The difference between the experimental $C_p(T)$ data and the Debye model fits below 100 K and 70 K for $PrCuAl_3$ and $NdCuAl_3$, respectively, arises due to the CEF contribution which is discussed below.

Figure 7(a) shows the magnetic contributions to the specific heat $C_{mag}(T)$ and entropy $S_{mag}(T)$ for $PrCuAl_3$. The magnetic contribution $C_{mag}(T)$ was obtained by subtracting the lattice contribution roughly equal to that of $LaCuAl_3$ from the $C_p(T)$ data of $PrCuAl_3$. The magnetic entropy $S_{mag}(T)$ was obtained by integrating the $C_{mag}(T)/T$ versus T plot. The basic feature of broad Schottky type anomaly observed in $C_{mag}(T)$ data

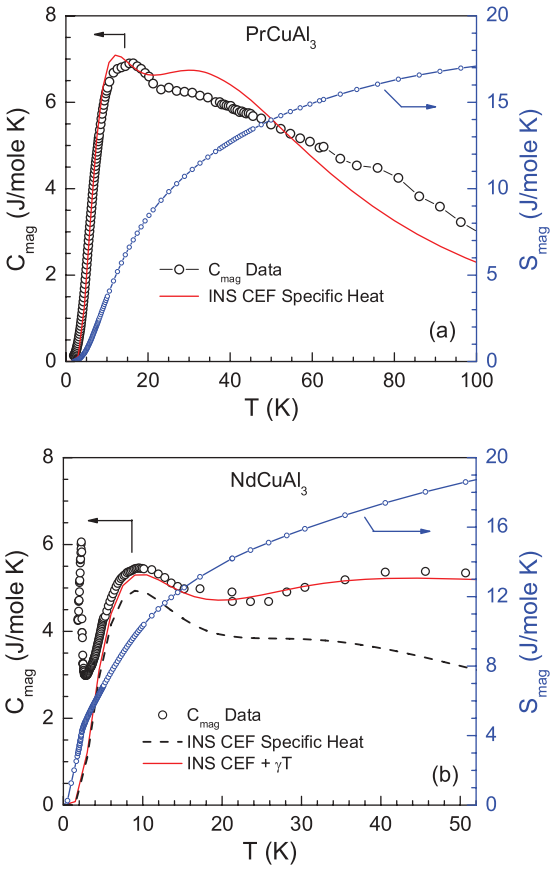

FIG. 7. (Color online) The temperature T dependence of magnetic contributions to the specific heat C_{mag} and entropy S_{mag} of (a) $PrCuAl_3$ and (b) $NdCuAl_3$. The solid curves represent the fits with the crystal field scheme obtained from the analysis of the inelastic neutron scattering data.

could be reasonably described by the crystal electric field model. The solid curve in Fig. 7(a) represents the specific heat data calculated for crystal field level scheme obtained from the analysis of inelastic neutron scattering data discussed below. The ground state is a singlet lying below the first excited doublet at 28 K, second excited singlet at 64 K, third excited singlet at 106 K, fourth excited singlet at 118 K, fifth excited singlet at 129 K, and sixth excited doublet at 157 K. The proposed crystal field level scheme is consistent with the temperature dependence of the magnetic entropy $S_{mag}(T)$ which attains a value of 1.15 R ln 3 at 28 K [see Fig. 7(a)], the excess entropy being the contribution from the higher states.

The magnetic contributions $C_{mag}(T)$ and $S_{mag}(T)$ to the specific heat and entropy of $NdCuAl_3$ are shown in Fig. 7(b). The $C_{mag}(T)$ data were obtained from the difference in specific heats of $NdCuAl_3$ and $LaCuAl_3$ and $S_{mag}(T)$ data were obtained by integrating the $C_{mag}(T)/T$ versus T plot. The Schottky type anomaly observed in the low temperature $C_{mag}(T)$ data is well reproduced by the crystal field model. The specific heat corresponding to the crystal field level scheme (five doublets at 0, 16, 37, 103, and 126 K) obtained from the analysis of inelastic neutron scattering data (discussed below) is shown by a dotted curve in Fig. 7(b). It is seen that the CEF specific heat deviates from the observed $C_{mag}(T)$ data, however, if a contribution from γT ($\gamma = 40$ mJ/mole K^2) term is added to CEF specific heat then the $C_{mag}(T)$ data are well represented [solid curve in Fig. 7(b)]. It seems that the additional γT is required to take care of improper subtraction of electronic contribution because of the difference in γ values of $NdCuAl_3$ and $LaCuAl_3$. However, the additional $\gamma = 40$ mJ/mole K^2 is more than the difference γ of $\approx$16 mJ/mole K^2 between $LaCuAl_3$ and $NdCuAl_3$ (obtained from high temperature fit above). The reason for why such a high value of γ is required to match the INS CEF heat capacity with the $C_{mag}(T)$ data is not clear. A CEF-split doublet ground state also follows from the T dependence of S_{mag} which attains a value of R ln 2 at 3.8 K [see Fig. 7(b)]. Further, the magnetic entropy attains a value of R ln 4 near 13 K supporting the first excited doublet state to be separated by about 16 K from the ground state. All these results of the temperature dependent magnetic entropy support the proposed crystal field level scheme obtained from the INS analysis (discussed below).

D. Inelastic neutron studies

The inelastic neutron scattering (INS) data were collected at 4.5 K with neutrons having incident energy $E_i = 11$ and 20 meV for scattering angles between 3° and 135°. Figures 8 and 9 show the color-coded contour map of the scattering intensity, energy transfer (E) versus momentum transfer (Q) spectra for inelastic neutron scattering at 4.5 K from $PrCuAl_3$ and $NdCuAl_3$, respectively for $E_i = 11$ and 20 meV. The spectra shown in Figs. 8 and 9 have been normalized in the absolute units (mb/sr/meV) using the scattering from the standard vanadium sample measured under the identical conditions. The presence of two sharp inelastic excitations near 2 and 9 meV are evident in the INS spectra of $PrCuAl_3$. However, for $NdCuAl_3$ we observe four transitions at 1.4, 3.2, 8.9, and 10.9 meV.

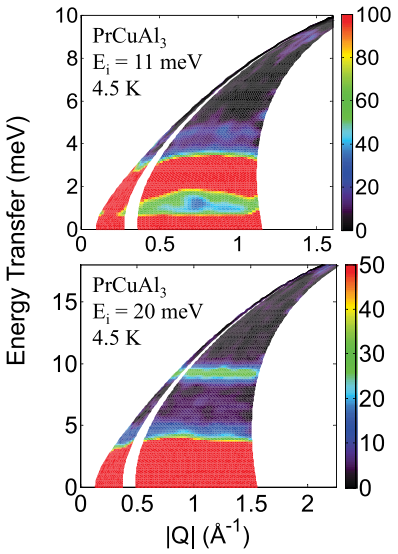

FIG. 8. (Color online) The color-coded contour map of inelastic neutron scattering intensity of $PrCuAl_3$ measured with incident energy $E_i = 11$ and 20 meV at 4.5 K plotted as a function of energy transfer (E) and wave vector transfer $|Q|$.

As shown in Fig. 10 the Q-dependent energy integrated intensity between 1.5 and 3.5 meV as well as between 8.5 and 10 meV at 4.5 K for $PrCuAl_3$ follows the Pr^{3+} magnetic form factor squared $[F^2(Q)]$ suggesting that the inelastic excitations in $PrCuAl_3$ result mainly from the single-ion CEF transitions. It should be noted that the INS peak near 2 meV shows dispersion, which is a typical effect of magnetic exchange (J_{ex}) interaction. Further the softens of the 2 meV peak as $Q \rightarrow 0$ may be taken as an indication of ferromagnetic type exchange, which is in agreement with the positive sign of θ_p observed from the magnetic susceptibility data. A very similar inelastic response has also been observed in the paramagnetic state of the cubic $PrInNi_4$ compound, which has a nonmagnetic doublet

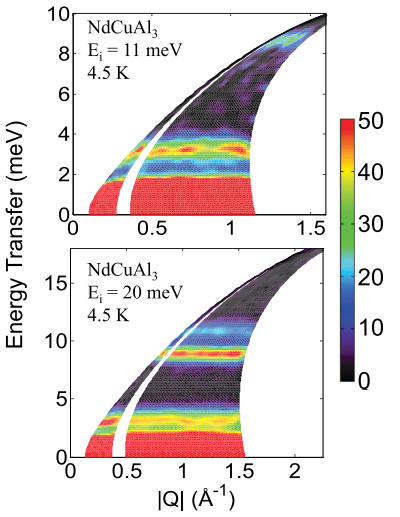

FIG. 9. (Color online) The color-coded contour map of inelastic neutron scattering intensity of $NdCuAl_3$ measured with incident energy $E_i = 11$ and 20 meV at 4.5 K plotted as a function of energy transfer (E) and wave vector transfer $|Q|$.

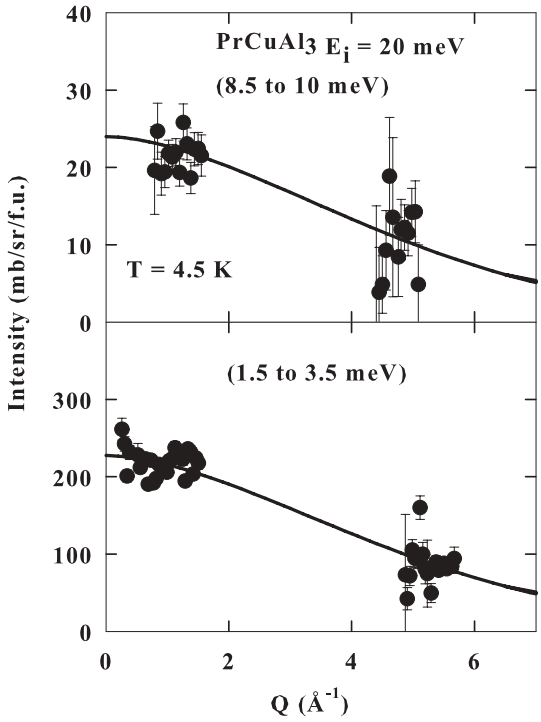

FIG. 10. The Q dependence of the energy integrated intensity of $PrCuAl_3$ integrated between 1.5 and 3.5 meV (bottom) as well as between 8.5 and 10 meV (top) at 4.5 K for incident energy $E_i = 20$ meV. The solid line represents the magnetic form factor squared for Pr^{3+} ion, scaled to the data.

ground state and the first excited state is a triplet separated by 1.7 meV.[34]

The Q-dependent integrated intensity between 2.5 and 4 meV, 8 and 9.6 meV, and 10 and 12 meV at 4.5 K for $NdCuAl_3$ is shown in Fig. 11, which, as expected, follows the square of Nd^{3+} magnetic form factor $[F^2(Q)]$: A slight deviation at high Q could be due to weak phonon contribution or background from the TCCR. This suggests that the inelastic excitations in $NdCuAl_3$ also result mainly from the single-ion CEF-transitions.

The $F^2(Q)$ behavior of Q-dependent integrated intensity in both the compounds also justifies our assumption of very small phonon contribution for $|Q| < 2$ which we have used for crystal field analysis. Further to avoid the problem of resolution mixing from the 4 m and 2.5 m banks of HET we have used the data from 2.5 m bank only in our CEF analysis. The use of 2.5 m bank (where the dispersions are weaker, see Figs. 8 and 9) also validates our analysis, which is based on the pure CEF model without considering the effect of magnetic exchange.

For unpolarized neutrons, the neutron scattering is given by,[35]

$$S(Q,\omega) = \frac{\hbar\omega}{1-\exp(-\hbar\omega/k_B T)} F^2(Q)\chi_0 P(Q,\hbar\omega), \quad (5)$$

where $F(Q)$ is the magnetic form factor of Pr^{3+} or Nd^{3+}, $P(Q,\hbar\omega)$ is the normalized spectral function (usually Lorentzian), and χ_0 is the static bulk susceptibility discussed later [Eqs. (9)–(11)]. Figures 12 and 14 show the INS spectra

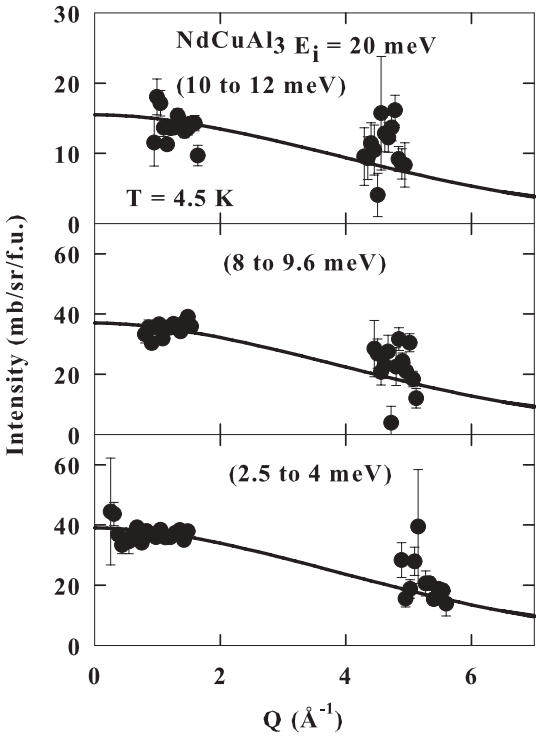

FIG. 11. The Q dependence of energy integrated intensity of $NdCuAl_3$ integrated between 2.5 and 4 meV, 8 and 9.6 meV, and 10 and 12 meV at 4.5 K for incident energy $E_i = 20$ meV. The solid line represents the magnetic form factor squared for Nd^{3+} ion, scaled to the data.

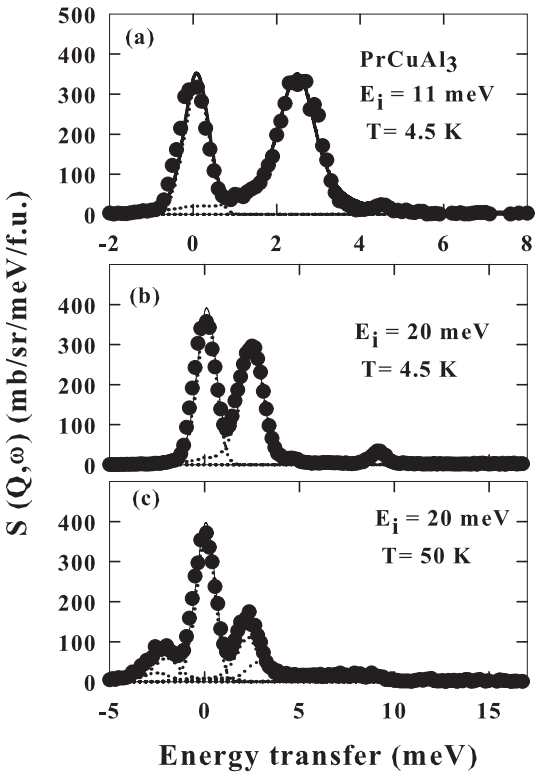

FIG. 12. The observed inelastic scattering of $PrCuAl_3$ at 4.5 K (for $E_i = 11$ and 20 meV). The solid line shows the fit based on the crystal field model. The dotted lines represent the different components.

TABLE III. Crystal field parameters B_n^m and splitting energies Δ of excited states (with respect to ground state, $\Delta_0 \equiv 0$) obtained from the refinement of the INS data of $PrCuAl_3$ and $NdCuAl_3$.

CEF Parameter	$PrCuAl_3$	$NdCuAl_3$
B_2^0 (meV)	$+0.156(2)$	$+0.063(2)$
B_4^0 (meV)	$-0.325(6) \times 10^{-2}$	$+0.75(1) \times 10^{-3}$
B_4^4 (meV)	$-0.175(5) \times 10^{-1}$	$-0.488(6) \times 10^{-2}$
B_6^0 (meV)	$-0.44(4) \times 10^{-5}$	$+0.189(1) \times 10^{-4}$
B_6^4 (meV)	$-0.13(2) \times 10^{-3}$	$+0.702(4) \times 10^{-3}$
Δ_1 (meV)	2.41	1.40
Δ_2 (meV)	5.49	3.19
Δ_3 (meV)	9.15	8.86
Δ_4 (meV)	10.17	10.87
Δ_5 (meV)	11.13	
Δ_6 (meV)	13.52	

for $PrCuAl_3$ and $NdCuAl_3$, respectively, in the form of scattering law $S(Q,\omega)$.

The inelastic response of $PrCuAl_3$ shown in Fig. 12 clearly demonstrates two well pronounced inelastic excitations centered around 2 and 9 meV which could be fitted with a model based on crystal electric field effect. In the tetragonal symmetry, point group (D_{4h}), the crystal field Hamiltonian for a rare earth (Pr or Nd) is given by

$$H_{\mathrm{CEF}} = B_2^0 O_2^0 + B_4^0 O_4^0 + B_4^4 O_4^4 + B_6^0 O_6^0 + B_6^4 O_6^4, \quad (6)$$

where O_n^m are the Stevens operator and B_n^m are the phenomenological crystal field parameters. In a tetragonal symmetry the crystal electric field removes the nine-fold degeneracy of $4f$ ground multiplet of Pr^{3+} ($J = 4$) splitting in five singlets ($\Gamma_{t1}^{(1)}$, $\Gamma_{t1}^{(2)}$, Γ_{t2}, Γ_{t3}, Γ_{t4}) and two doublets ($\Gamma_{t5}^{(2)}$, $\Gamma_{t5}^{(1)}$), where the Γ_j's are the irreducible representations of the point group. We have made a simultaneous fit to $E_i = 11$ meV and 20 meV data at 4.5 K. The solid line in Fig. 12 represents the fit by CEF model to the observed inelastic scattering data of $PrCuAl_3$. The phenomenological crystal field parameters B_n^m obtained from the simultaneous fit of 11 meV and 20 meV INS data at 4.5 K are listed in Table III. However, the INS data at 50 K could not be fitted very well by the same set of B_n^m parameters. A very small change in the energy of excitations has been observed at 50 K compared with 4.5 K. At $Q = 0$ the peak energy increases from 2 meV (at 4.5 K) to 2.2 meV (at 50 K), but at $Q = 0.75$ (0.7–0.8 Å) the peak energy decreases from 2.7 meV (at 4.5 K) to 2.55 meV (at 50 K). This observation is consistent with the expected behavior from random phase approximation (RPA). Therefore in order to fit the 50 K INS data for $E_i = 20$ meV with the CEF model we have to vary B_n^m parameters. A reasonable fit to 50 K data is obtained for slightly different value of CEF parameter $B_0^4 = -0.292(4) \times 10^{-2}$ with all other B_n^m parameters fixed to that in Table III.

The CEF wave functions and the CEF level scheme corresponding to the B_n^m parameters obtained from the simultaneous fit of 11 meV and 20 meV INS data at 4.5 K (Table III) are shown in Fig. 13. The ground state is a singlet, and the first excited state doublet is at 28 K. It has been found that for a singlet ground state, the system exhibits magnetic order only above a critical value of J_{ex}/Δ, where J_{ex} is the Heisenberg exchange interaction and Δ is the crystal field splitting energy

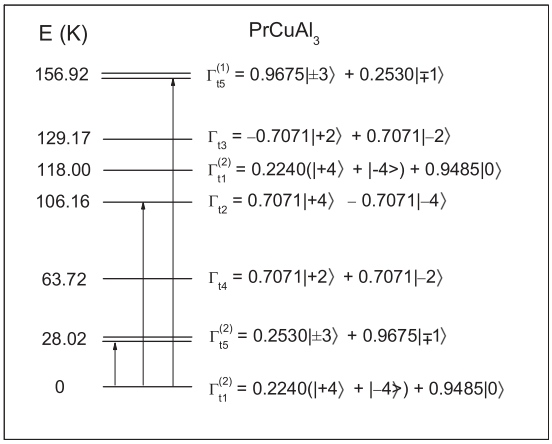

FIG. 13. Crystal electric field level scheme and f-electron wave functions of Pr^{3+} ions in $PrCuAl_3$ deduced from the CEF model of inelastic neutron scattering experiment. The transitions from the ground state to the excited states that contribute to the observed excitations are shown by arrows.

between the ground state and the excited state.[36,37] The absence of the long range ordering down to 1.8 K may indicate that the mean-field critical temperature, where the self-induced moment forms spontaneously, is below 1.8 K for $PrCuAl_3$.[37]

The mean-field critical temperature below which the self-induced moment may form spontaneously in a singlet-doublet system can be estimated by[38]

$$T_c = \Delta \left\{ \ln \left[\frac{J_{ex}\alpha^2 + n\Delta}{J_{ex}\alpha^2 - n\Delta} \right] \right\}^{-1}, \tag{7}$$

where $n = 2$ is the degeneracy of the excited state and α is the matrix element between the ground state singlet and excited state doublet. For $PrCuAl_3$ $\alpha^2 = 12.12$ and $\Delta = 2.41$ meV (=28 K). J_{ex} can be estimated from the Weiss temperature by using the relation

$$\theta_p = -\frac{z J_{ex} J(J+1)}{3k_B}, \tag{8}$$

where z is the coordination number and J is the total angular momentum quantum number. For Pr^{3+} $J = 4$ and $z = 4$ in $BaNiSn_3$-type tetragonal structure of $PrCuAl_3$. From the magnetic susceptibility data we have found $\theta_p = +19$ K, thus from Eq. (8) we obtain $J_{ex} = -0.7125$ K. However, to obtain a nonzero T_c from Eq. (7) a necessary condition is $J_{ex}\alpha^2 - n\Delta > 0$ or $J_{ex} > n\Delta/\alpha^2 = 4.62$ K, which is not satisfied by the above value of J_{ex}. This suggests that there is no spontaneous induced moment ordering in $PrCuAl_3$.

As seen from Fig. 14, four sharp inelastic excitations at 1.4, 3.2, 8.9, and 10.9 meV are evident in the inelastic response of $NdCuAl_3$. The observed INS spectra are well represented by the CEF model shown in Fig. 15. The solid lines in Fig. 14 represent the simultaneous fit of 11 meV and 20 meV data. The crystal field parameters B_n^m obtained from the CEF analysis of INS data of $NdCuAl_3$ are listed in Table III. The corresponding crystal field level scheme and electronic wave functions are shown in Fig. 15. The ground state is a doublet, and the excited state doublets are situated at 16.20, 36.96, 102.82, and 126.11 K.

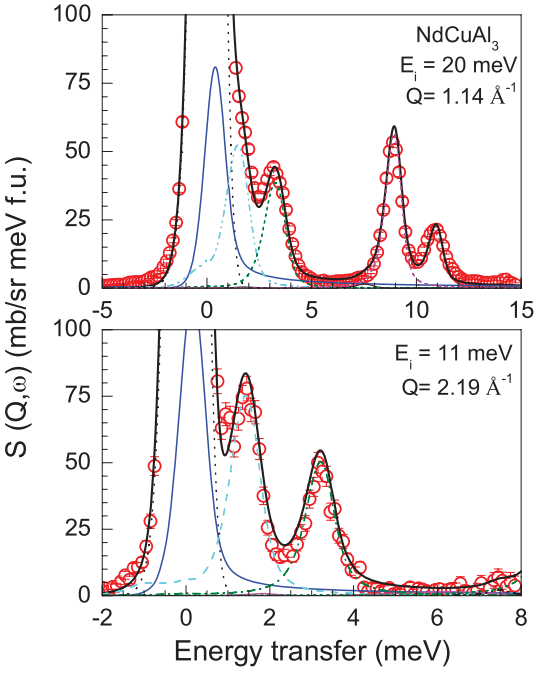

FIG. 14. (Color online) The observed inelastic scattering of $NdCuAl_3$ at 4.5 K (for $E_i = 11$ and 20 meV). The solid line shows the fit based on the crystal field model. The dashed and dash-dotted lines represent the different components.

Using the CEF level schemes shown in Figs. 13 and 15 we have calculated the specific heat of $PrCuAl_3$ and $NdCuAl_3$. The CEF calculated specific heats using the software AMOS are shown in Figs. 7(a) and 7(b) for $PrCuAl_3$ and $NdCuAl_3$, respectively. As discussed above, the INS CEF specific heats represent well the magnetic contribution to specific heats $C_{mag}(T)$. This further supports the validity of proposed CEF schemes. Further we have calculated the magnetic susceptibility $\chi(T)$ and ground state moment using the CEF parameters obtained from the fit of INS data. In order to calculate $\chi(T)$ from INS data, the static susceptibility χ_0 due to the CEF

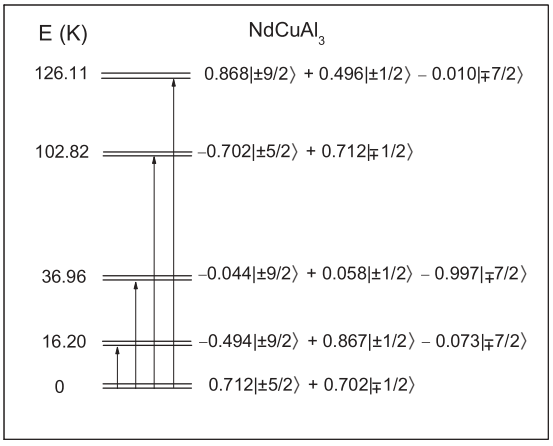

FIG. 15. Crystal electric field level scheme and f-electron wave functions of Nd^{3+} ions in $NdCuAl_3$ deduced from the analysis of the INS data based on the CEF model. The transitions from the ground state to the excited states that contribute to the observed excitations are shown by arrows.

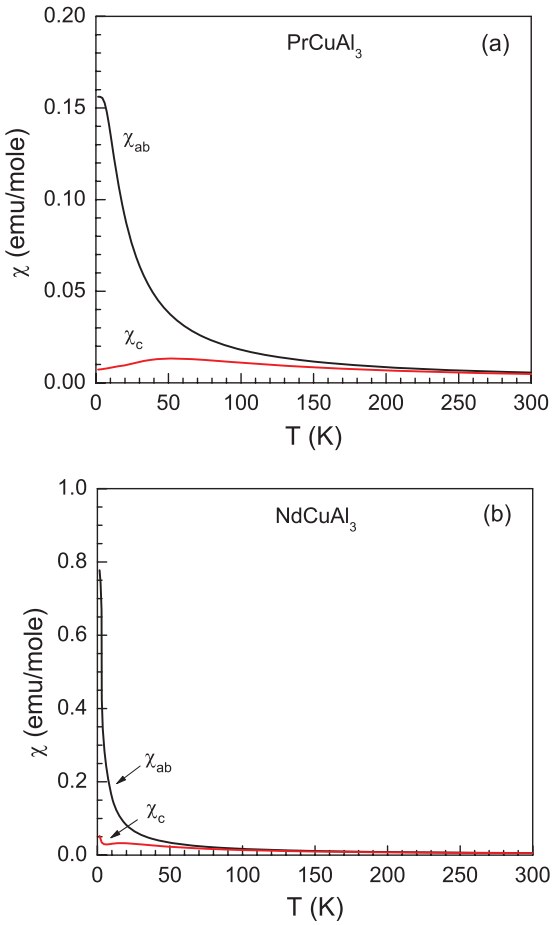

FIG. 16. (Color online) The calculated single crystal susceptibility $\chi(T)$ of (a) $PrCuAl_3$ and (b) $NdCuAl_3$ using CEF parameters given in Table III.

transitions in Eq. (5) can be written as the sum of Curie (χ_C) and Van Vleck (χ_{VV}) susceptibilities, i.e.,[35]

$$\chi_0 = \sum_m \chi_C^m + \sum_{m \neq n} \chi_{VV}^{mn} \tag{9}$$

with

$$\chi_C^m = \frac{g_J^2 \mu_B^2}{k_B T} \rho_m \sum_{\alpha=x,y,z} |\langle m|J^\alpha|m\rangle|^2 \tag{10}$$

and

$$\chi_{VV}^{mn} = 2 g_J^2 \mu_B^2 (\rho_n - \rho_m) \frac{\sum_{\alpha=x,y,z} |\langle m|J^\alpha|n\rangle|^2}{\Delta_{mn}}, \tag{11}$$

where $\rho_m = \exp(-E_m/k_B T)/Z$ is the population of CEF level with wave function $|m\rangle$ and energy eigenvalue E_m (Z being the partition function), J^α represents the x, y, or z component of the angular momentum operator, and $\Delta_{mn} = E_n - E_m$ is the splitting energy between the levels $|m\rangle$ and $|n\rangle$.

The single crystal $\chi(T)$ calculated for CEF transitions using the software AMOS is shown in Figs. 16(a) and 16(b) for $PrCuAl_3$ and $NdCuAl_3$, respectively. For $PrCuAl_3$ the calculated single crystal $\chi(T)$ reveals strong anisotropy with easy axis in the ab plane, i.e., $\chi_{ab} > \chi_c$ where χ_{ab} and χ_c are the susceptibilities for applied field $H \parallel ab$ and $H \parallel c$, respectively. The χ_c exhibits a broad peak near 50 K, while χ_{ab} shows saturation type behavior below 5 K. The calculated single crystal $\chi(T)$ of $NdCuAl_3$ also reveals strong anisotropy with the easy axis in the ab plane (i.e., $\chi_{ab} > \chi_c$). The χ_c exhibits a broad peak near 18 K, while χ_{ab} shows a Curie-type rise at low temperature, which agrees with a finite value of the ground state moment.

IV. CONCLUSIONS

The structural, magnetic, and thermal properties of ternary intermetallic compounds $PrCuAl_3$ and $NdCuAl_3$ have been investigated using various experimental techniques. No magnetic or superconducting phase transition is observed in $PrCuAl_3$ down to 1.8 K at ambient pressure. In contrast, an antiferromagnetic ordering with $T_N = 2.35$ K is observed in $NdCuAl_3$. An analysis of the specific heat and inelastic neutron scattering data reveals a singlet ground state for $PrCuAl_3$ and a doublet ground state for $NdCuAl_3$. All the observed inelastic excitations, at 2 and 9 meV in $PrCuAl_3$, and at 1.4, 3.2, 8.9, and 10.9 meV in $NdCuAl_3$ could be explained on the basis of the CEF model which allowed us to evaluate the crystal electric field parameters and hence the crystal field level scheme and electronic wave functions for Pr^{3+} and Nd^{3+} ions in these compounds. The absence of any clear additional CEF peak than that expected based on the CEF model indicates the very weak CEF-phonon (or magnetoelastic) coupling in these compounds in contrast to the strong one found in $CeCuAl_3$. Pressure study on these compounds to see the pressure induced superconductivity with noncentrosymmetric structure should be desired.

ACKNOWLEDGMENTS

Authors would like to acknowledge financial assistance from CMPC-STFC Grant No. CMPC-09108. We thank W. Kockelmann for carrying out the neutron diffraction measurements on the ROTAX diffractometer at 300 K.

*devashibhai.adroja@stfc.ac.uk
†Present address: Ames Laboratory, Department of Physics and Astronomy, Iowa State University, Ames, Iowa 50011, USA; vivekkranand@gmail.com

[1] V. M. Edel'stein, Sov. Phys. JETP **68**, 1244 (1989).
[2] L. P. Gor'kov and E. I. Rashba, Phys. Rev. Lett. **87**, 037004 (2001).
[3] K. V. Samokhin, E. S. Zijlstra, and S. K. Bose, Phys. Rev. B **69**, 094514 (2004).
[4] P. A. Frigeri, D. F. Agterberg, A. Koga, and M. Sigrist, Phys. Rev. Lett. **92**, 097001 (2004).

[5]S. Fujimoto, J. Phys. Soc. Jpn. **76**, 051008 (2007).
[6]E. Bauer, G. Hilscher, H. Michor, C. Paul, E. W. Scheidt, A. Gribanov, Y. Seropegin, H. Noel, M. Sigrist, and P. Rogl, Phys. Rev. Lett. **92**, 027003 (2004).
[7]E. Bauer, H. Kaldarar, A. Prokofiev, E. Royanian, A. Amato, J. Sereni, W. Bramer-Escamilla, and I. Bonalde, J. Phys. Soc. Jpn. **76**, 051009 (2007).
[8]Y. Muro, D. Eom, N. Takeda, and M. Ishikawa, J. Phys. Soc. Jpn. **67**, 3601 (1998).
[9]N. Kimura, K. Ito, K. Saitoh, Y. Umeda, H. Aoki, and T. Terashima, Phys. Rev. Lett. **95**, 247004 (2005).
[10]Y. Muro, M. Ishikawa, K. Hirota, Z. Hiroi, N. Takeda, N. Kimura, and H. Aoki, J. Phys. Soc. Jpn. **76**, 033706 (2007).
[11]N. Kimura, Y. Muro, and H. Aoki, J. Phys. Soc. Jpn. **76**, 051010 (2007).
[12]I. Sugitani, Y. Okuda, H. Shishido, T. Yamada, A. Thamizhavel, E. Yamamoto, T. D. Matsuda, Y. Haga, T. Takeuchi, R. Settai, and Y. Onuki, J. Phys. Soc. Jpn. **75**, 043703 (2006).
[13]Y. Okuda, Y. Miyauchi, Y. Ida, Y. Takeda, C. Tonohiro, Y. Oduchi, T. Yamada, N. D. Dung, T. D. Matsuda, Y. Haga, T. Takeuchi, M. Hagiwara, K. Kindo, H. Harima, K. Sugiyama, R. Settai, and Y. Ōnuki, J. Phys. Soc. Jpn. **76**, 044708 (2007).
[14]Y. Tada, N. Kawakami, and S. Fujimoto, Phys. Rev. B **81**, 104506 (2010).
[15]V. K. Pecharsky, O.-B. Hyun, and K. A. Gschneidner, Jr., Phys. Rev. B **47**, 11839 (1993).
[16]A. Thamizhavel, T. Takeuchi, T. D. Matsuda, Y. Haga, K. Sugiyama, R. Settai, and Y. Onuki, J. Phys. Soc. Jpn. **74**, 1858 (2005).
[17]R. Settai, I. Sugitani, Y. Okuda, A. Thamizhavel, M. Nakashima, Y. Onuki, and H. Harima, J. Magn. Magn. Mater. **310**, 844 (2007).
[18]M. A. Continentino, S. N. de Medeiros, M. T. D. Orlando, M. B. Fontes, and E. M. Baggio-Saitovitch, Phys. Rev. B **64**, 012404 (2001).
[19]V. V. Krishnamurthy, K. Nagamine, I. Watanabe, K. Nishiyama, S. Ohira, M. Ishikawa, D. H. Eom, T. Ishikawa, and T. M. Briere, Phys. Rev. Lett. **88**, 046402 (2002).
[20]V. K. Anand, A. D. Hillier, D. T. Adroja, A. M. Strydom, H. Michor, K. A. McEwen, and B. D. Rainford, Phys. Rev. B **83**, 064522 (2011).
[21]V. K. Anand, D. T. Adroja, A. D. Hillier, J. Taylor, and G. Andŕe, Phys. Rev. B **84**, 064440 (2011).
[22]F. Hulliger, J. Alloys Comp. **218**, 255 (1995).
[23]S. A. Mentink, N. M. Bos, B. J. van Rossum, G. J. Nieuwenhuys, J. A. Mydosh, and K. H. J. Buschow, J. Appl. Phys. **73**, 6625 (1993).
[24]M. Kontani, H. Ido, H. Ando, T. Nishioka, and Y. Yamaguchi, J. Phys. Soc. Jpn. **63**, 1652 (1994).
[25]S. Mock, C. Pfleiderer, and H. v. Lohneysen, J. Low Temp. Phys. **115**, 1 (1999).
[26]M. Kontani, N. Sugihara, K. Murase, and N. Môri, Czech. J. Phys. **46**, 2067 (1996).
[27]T. Nishioka, Y. Kawamura, H. Kato, M. Matsumura, K. Kodama, and N. K. Sato, J. Magn. Magn. Mater. **310**, e12 (2007).
[28]Y. Kawamura, T. Nishioka, H. Kato, M. Matsumura, and K. Kodama, J. Phys.: Conf. Ser. **150**, 042088 (2009).
[29]Y. Kawamura, T. Nishioka, H. Kato, M. Matsumura, K. Matsubayashi, and Y. Uwatoko, J. Phys.: Conf. Ser. **200**, 012082 (2010).
[30]D. T. Adroja, A. del Moral, C. de la Fuente, A. Fraile, E. A. Goremychkin, J. W. Taylor, A. D. Hillier, and F. Fernandez-Alonso, Phys. Rev. Lett. **108**, 216402 (2012).
[31]C. Kittel, *Introduction to Solid State Physics*, 8th ed. (Wiley, New York, 2005).
[32]E. S. R. Gopal, *Specific Heats at Low Temperatures* (Plenum, New York, 1966).
[33]R. J. Goetsch, V. K. Anand, A. Pandey, and D. C. Johnston, Phys. Rev. B **85**, 054517 (2012).
[34]H. C. Walker, K. A. McEwen, D. T. Adroja, J.-G. Park, Y. S. Kwon, J.-Y. So, W. Kockelmann, and M. Meissner, Physica B **385-386**, 41 (2006).
[35]E. Holland-Moritz, D. Wohlleben, and M. Loewenhaupt, Phys. Rev. B **25**, 7482 (1982).
[36]J. Jensen and A. R. Mackintosh, *Rare Earth Magnetism: Structures and Excitations* (Oxford University Press, Oxford, 1991).
[37]B. R. Cooper, Phys. Rev. **163**, 444 (1967).
[38]E. A. Goremychkin, R. Osborn, B. D. Rainford, R. T. Macaluso, D. T. Adroja, and M. Koza, Nat. Phys. **4**, 766 (2008).